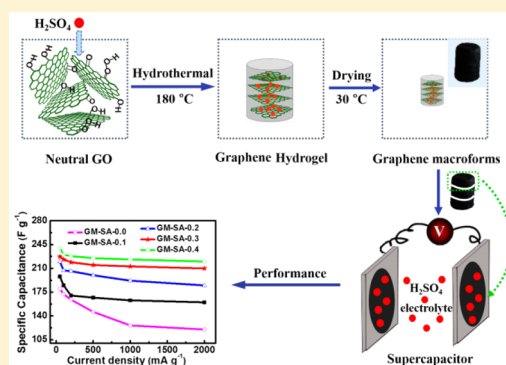


# Dense 3D Graphene Macroforms with Nanotuned Pore Sizes for High Performance Supercapacitor Electrodes

Jiangying Qu,<sup>\*,†,‡</sup> Yuqian Li,<sup>†</sup> Siyuan Lv,<sup>†</sup> Feng Gao,<sup>†,‡</sup> Chuang Geng,<sup>†</sup> and Mingbo Wu<sup>\*,§</sup><sup>†</sup>Faculty of Chemistry and Chemical Engineering, Liaoning Normal University, Dalian 116029, China<sup>‡</sup>Carbon Research Laboratory, Center for Nano Materials and Science, School of Chemical Engineering, State Key Lab of Fine Chemicals, Dalian University of Technology, Dalian 116024, China<sup>§</sup>State Key Laboratory of Heavy Oil Processing, China University of Petroleum, Qingdao 266580, China

## S Supporting Information

**ABSTRACT:** Dense 3D graphene macroforms with nanotuned pore sizes have been synthesized using graphene oxide as the precursor and aqueous H<sub>2</sub>SO<sub>4</sub> as the mediator by coupling the hydrothermal method with an evaporation drying process. Depending on the contents of concentrated H<sub>2</sub>SO<sub>4</sub> trapped in the resultant carbons, the pore size of graphene macroforms in the range of about 0.5–4.8 nm can be obtained. The results indicate that liquid H<sub>2</sub>SO<sub>4</sub> trapped in graphene macroforms can act as the spacer of wrinkled graphene sheets, the catalyst of the dehydration, and the electrolyte of the supercapacitor. The pore sizes of the carbons play an important role in the electrochemical performances when used as the supercapacitor electrodes. The graphene macroform with an average pore size of 4.8 nm is an excellent electrode material in H<sub>2</sub>SO<sub>4</sub> electrolyte. Its specific capacitance is up to 230 F g<sup>-1</sup> at the current density of 0.1 A g<sup>-1</sup>, and the specific energy density and power density are up to 8.3 Wh kg<sup>-1</sup> and 1000 W kg<sup>-1</sup> in a two-electrode cell, respectively. The good electrochemical properties of as-made carbons may be attributed to the highly efficient ion transport channels in H<sub>2</sub>SO<sub>4</sub>-mediated graphene macroforms.



## 1. INTRODUCTION

Graphene as the monolayer of graphite has attracted much interest in recent years because of its unique two-dimensional (2D) structures and excellent physical and chemical properties.<sup>1–3</sup> Up to now, various effective techniques including chemical vapor deposition (CVD)<sup>4–8</sup> and mechanical<sup>9–11</sup> or chemical exfoliations<sup>12–15</sup> have been developed for the synthesis of graphene. It is well recognized that the assembly of 2D graphene sheets into 3D architectures will pave a new way for achieving high-performance graphene-based materials.<sup>16–24</sup> In this field, Chen et al. synthesized the foam-like graphene macroforms (GMs) with high electrical conductivity and large specific surface area by CVD.<sup>4</sup> Another approach to get GMs is the self-assembly of chemically modified graphene in solution starting from graphene oxide (GO)<sup>21–24</sup> or reduced GO (rGO).<sup>18–20</sup> In this field, one of the simplest methods is the self-assembly of 3D rGO gels in water or organic solvents, where the force balance between electrostatic repulsion and interplanar van der Waals interaction dominates its formation.<sup>25–29</sup> To achieve 3D microstructures with good mechanical strength, a further freeze-drying process to remove the trapped water for the fabrication of aerogels is indispensable.<sup>30–35</sup> For example, Tang et al. prepared a rGO interconnected network via the hydrothermal process with the assistance of noble metal nanocrystals.<sup>34</sup> Tao et al. reported the production of reduced expanded porous graphene aerogel by the linkage of function-

alized graphene sheets with poly(vinyl alcohol) as the linker under hydrothermal conditions followed by a freeze-drying process.<sup>35</sup> Similarly, an aqueous GO suspension with appropriate concentration was directly submitted to hydrothermal treatment for the formation of rGO hydrogel in the absence of any reagents.<sup>36–38</sup> In general, the *in situ* formed graphene aerogel can be assembled into a 3D network with pore sizes ranging from submicrometer to several micrometers.<sup>24</sup> However, such porous structures predominated by macropores in the graphene aerogels limit their practical applications in many micropore- and/or mesopore-dependent fields in spite of the hydrothermal method being more simple and less costly compared with CVD.<sup>27</sup> For example, the large space of the graphene materials leads to the low packing density which is not effective for storing ions.<sup>30–33</sup> On the basis of the above-mentioned problems, Tao et al. produced compactly interlinked graphene sheets with the hierarchical micro/mesoporous structures and high density by an evaporation-induced drying of a graphene hydrogel, and this material exhibited an excellent volumetric capacitance (up to 376 F cm<sup>-3</sup>) for electrochemical capacitors.<sup>29</sup> Different from Tao's work, Yang et al. reported liquid electrolyte-mediated graphene

Received: July 10, 2015

Revised: September 24, 2015

Published: October 8, 2015

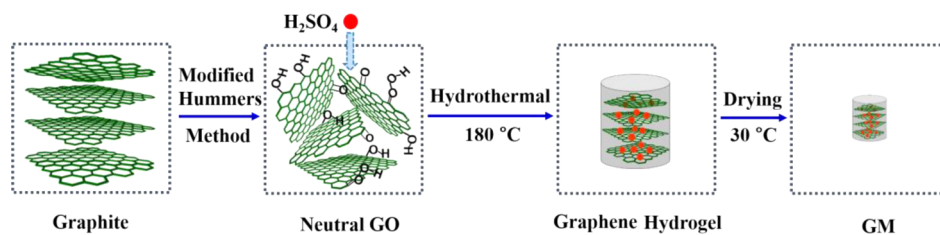


**Figure 1.** Schematic illustration of the self-assembly of the  $\text{H}_2\text{SO}_4$ -mediated 3D hydrogel and corresponding GM after the evaporation drying.

films with metastable and adaptive porous structures through a filtration–exchange–evaporation process.<sup>36</sup> In that work, graphene film was produced using graphene dispersion as the precursor exchanged with a miscible mixture of volatile and nonvolatile liquids followed by selective removal of the volatile liquid through vacuum evaporation. When used as a compact capacitive energy storage, the resulting films obtained volumetric energy densities approaching  $60 \text{ Wh L}^{-1}$  with EMIMBF<sub>4</sub>/AN as the electrolyte. Nevertheless, the fabrication of GMs with more controllable porous structures to suit different applications is still a challenging work.<sup>29,36</sup>

Recently, the synthesis of graphene has been widely studied using acid such as hydrohalic acid (HI) and  $\text{H}_2\text{SO}_4$  as effective chemical reducing agents. For example, Pei et al. reported the HI reducing method to reduce GO films into highly conductive graphene films without destroying their integrity and flexibility at low temperature based on the nucleophilic substitution reaction.<sup>39</sup> Similarly, Zhang et al. also reported the synthesis of graphene hydrogels through hydrothermal treatment of GO dispersions followed by the reduction of hydrazine or HI.<sup>40</sup> Though the reported work has demonstrated that HI is a good reducing agent to improve the conductivity of the graphene, its expensive price and poor stability in air limit its wide application. Alternatively, Hong et al. reported the synthesis of graphene by rapid reduction and expansion exfoliation of  $\text{H}_2\text{SO}_4$ -intercalated GO in ambient atmosphere, and the specific capacitance of the obtained graphene powder reached  $216 \text{ F g}^{-1}$  at  $2 \text{ A g}^{-1}$  in a three-electrode cell. It was found that  $\text{H}_2\text{SO}_4$  as the catalyst could remove the oxygenic and hydric groups of GO through dehydration.<sup>41</sup> In spite of those efforts, the role of the acid agent in the fabrication of graphene-based materials for electrochemical applications needs to be further explored.

Herein, we report the synthesis of GMs with finely tailored micro/mesopores by the *in situ* hydrothermal method followed by an evaporation drying process using GO as the precursor and aqueous  $\text{H}_2\text{SO}_4$  as both the mediator and the catalyst. Different from the traditional hard and soft template methods for synthesis of porous carbons, the selective removal of water leads to the shrinkage of 3D hydrogels by the capillary compression, and the concentrated  $\text{H}_2\text{SO}_4$  trapped in the GMs after the evaporation of water plays an important role in tailoring of their pore sizes. More promising, the shaped GMs could be fabricated directly as an electrode for the assembly of a supercapacitor device free of any additives due to their acceptable conductivity. The supercapacitor performances of the resulting carbons are investigated.

## 2. EXPERIMENTAL SECTION

**2.1. Preparation of  $\text{H}_2\text{SO}_4$ -Mediated GMs.** The GO was synthesized from natural graphite powder based on a modified Hummers method according to our previous work.<sup>42,43</sup> For the

preparation of GMs, 5.0 mL of the homogeneous GO suspension ( $7.2 \text{ mg mL}^{-1}$ ) was sonicated for 1 h under room temperature. Then 10.0 mL of aqueous sulfuric acid (SA) with different concentrations ( $0.1\text{--}0.4 \text{ mol L}^{-1}$ ) was dropwise added into the above solution and stirred for 0.5 h. The obtained homogeneous GO/SA colloidal suspension was placed in a 20 mL Teflon-lined autoclave and hydrothermally treated at  $180 \text{ }^\circ\text{C}$  for 15 h, resulting in a black cylindrical hydrogel. The collected hydrogels were dried at room temperature under the air atmosphere to produce GMs. The as-synthesized samples were denoted as GM-SA-X, where X represented the concentration of  $\text{H}_2\text{SO}_4$  used for the synthesis of hydrogels.

**2.2. Electrochemical Measurements.** The electrochemical properties of as-obtained GMs were investigated at room temperature. The slices (each with a thickness of about 2–5 mm) were cut from the  $\text{H}_2\text{SO}_4$ -mediated graphene cylindrical hydrogel and subjected to vacuum drying at room temperature. One dried slice of the GMs with a weight of about 2–3 mg was pressed onto a titanium mesh current collector to make one electrode. Then the symmetrical supercapacitor was assembled with a polypropylene membrane sandwiched between two electrodes. Before the electrochemical test, the as-prepared supercapacitor was soaked overnight in  $1.0 \text{ mol L}^{-1}$   $\text{H}_2\text{SO}_4$  electrolyte. The specific capacitance of the symmetrical supercapacitors was calculated from the discharge curves according to the equation of  $C_s = 2I \times \Delta t / (\Delta V \times m)$ ,<sup>29</sup> where  $C_s$  is the gravimetric capacitance of the electrode;  $I$  is the discharge current (A);  $\Delta t$  is the discharge time (s);  $\Delta V$  is the potential window (V) within the discharge time; and  $m$  (g) is the mass of a single electrode. The energy density ( $E$ ) and power density ( $P$ ) derived from the charge–discharge curves are calculated by the following equations:  $E = C_s \Delta V^2 / 28.8 \text{ Wh kg}^{-1}$  and  $P = 3600 \times E / t \text{ W kg}^{-1}$ ,<sup>29</sup> where  $C_s$  is the gravimetric capacitance of the electrode and  $\Delta V$  is the potential window (V) within the discharge time.

Both the cyclic voltammetry (CV) and the electrochemical impedance spectroscopy (EIS) were conducted on a CHI 660E electrochemical workstation (Chenhua, Shanghai, China). The galvanostatic charge–discharge measurement was performed on a Land Battery workstation at room temperature (Wuhan Land Instrument Company, China). The morphologies and structures of the as-obtained products were examined using field emission scanning electron microscopy (SEM, Hitachi Ltd. SU8010), powder X-ray diffraction (XRD, Rigaku D/max-2500 diffractometer with Cu  $K\alpha$  radiation), and X-ray photoelectron spectroscopy (XPS, Thermo VG Scientific Sigma Probe spectrometer). The Brunauer–Emmett–Teller (BET) surface area of as-synthesized samples was determined by  $\text{N}_2$  adsorption at 77 K using a Micromeritics ASAP 2020 analyzer, and the samples after removal of  $\text{H}_2\text{SO}_4$  were freeze-dried before measurement.

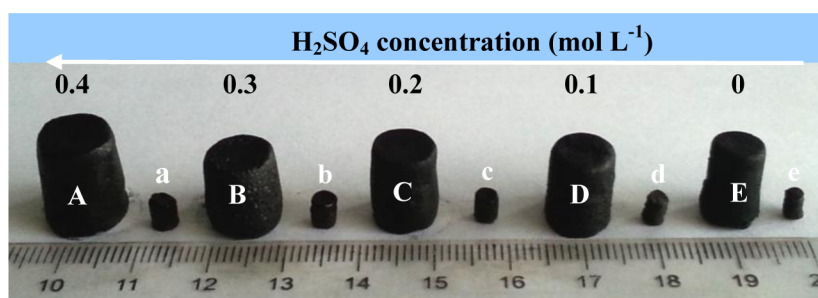


Figure 2. Photographs of  $\text{H}_2\text{SO}_4$ -mediated graphene hydrogels (A–E) and evaporation-induced GMs (a–e) with different sizes.

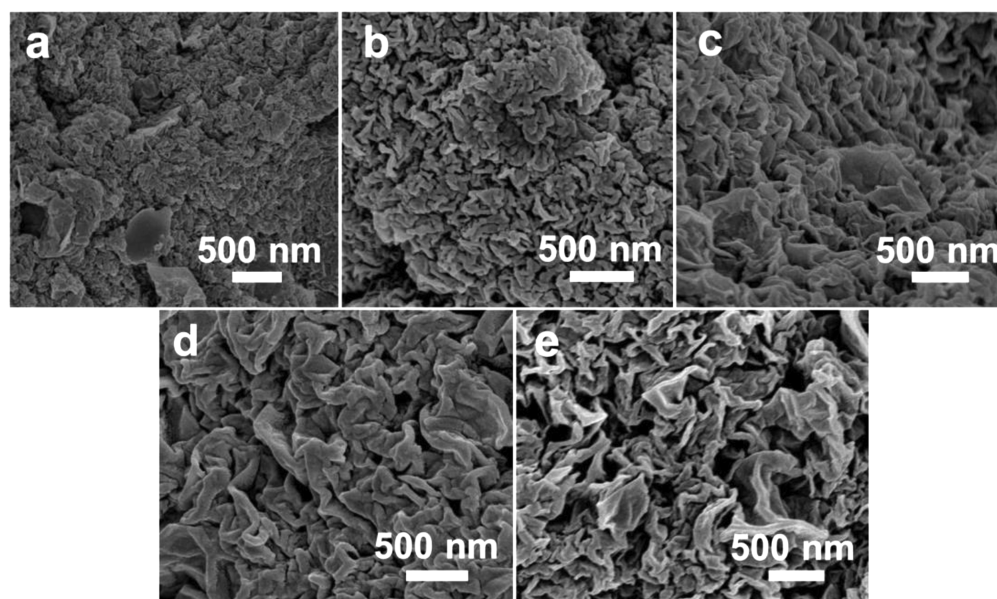


Figure 3. SEM images of the obtained GM samples: (a) GM-SA-0.0, (b) GM-SA-0.1, (c) GM-SA-0.2, (d) GM-SA-0.3, and (e) GM-SA-0.4.

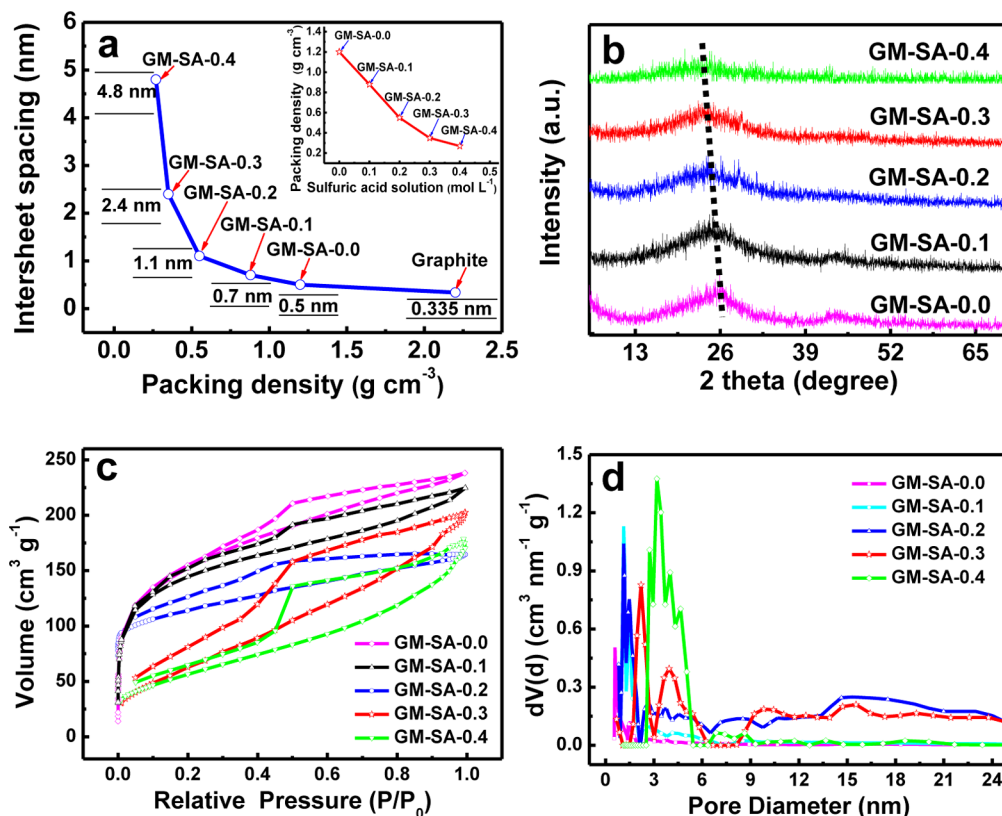
### 3. RESULTS AND DISCUSSION

Figure 1 illustrates the strategy for the synthesis of  $\text{H}_2\text{SO}_4$ -mediated GMs by the self-assembly of graphene hydrogels through coupling of the hydrothermal method with the evaporation drying process. Initially, neutral GO was prepared by the modified Hummers method using natural graphite as the carbon source.  $\text{H}_2\text{SO}_4$ -mediated graphene hydrogels were then self-assembled from GO with fixed concentration and  $\text{H}_2\text{SO}_4$  with different concentrations by the *in situ* hydrothermal method. Different from the reported freeze-drying technique,<sup>26,33</sup> evaporation drying was carried out to synthesize GMs with tailored micro/mesopores and high packing densities, which may have potential advantages as supercapacitor electrodes.

Figure 2 shows the photographs of the final products of  $\text{H}_2\text{SO}_4$ -mediated GMs. As shown in Figure 2A–E, 3D hydrogels with different sizes are obtained by hydrothermal treatment of GO suspension with the assistance of different concentrations of  $\text{H}_2\text{SO}_4$  solution; i.e., the higher the concentration of  $\text{H}_2\text{SO}_4$  solution, the larger the volume of the hydrogels. Accordingly, the different volume of the resultant hydrogels is mainly determined by the ratio of  $\text{H}_2\text{SO}_4$  and  $\text{H}_2\text{O}$  molecules. However, 3D hydrogel is difficult for assembly when the concentration of  $\text{H}_2\text{SO}_4$  is higher than  $0.4 \text{ mol L}^{-1}$  because of the negative effect of strong acid condition on the synthesis.<sup>25</sup> Furthermore, it is widely reported that freeze-drying can fix the 3D network of hydrogel in a spongy assembly

without obvious shrinkage.<sup>30,33</sup> By comparison, evaporation-induced drying produces stiff rod-like material with the volume shrinkage of  $1/8$ – $1/6$  based on its parent hydrogel, as shown in Figure 2a–e. During this process, the 3D hydrogel with macropores is compressed irreversibly by capillary pressure to shrink its pore sizes through selective removal of volatile  $\text{H}_2\text{O}$  trapped in the gel, while the GM is still solvated by the unvolatile  $\text{H}_2\text{SO}_4$  during the whole process. The degree of such volume shrinkage depends on the amount of unvolatile  $\text{H}_2\text{SO}_4$  retained in the GM; i.e., the larger the amount of  $\text{H}_2\text{SO}_4$  that remains, the larger the volume of GM. The surface morphologies of the obtained GMs are further investigated by SEM analysis, as shown in Figure 3a–e. SEM images reveal that wrinkled and sheet-like structures of GMs with different  $\text{H}_2\text{SO}_4$  concentration produce interlinked nanopores (Figure 3), which indicates that liquid  $\text{H}_2\text{SO}_4$  trapped in GMs can act as spacers to efficiently prevent the restacking of graphene sheets. The sizes of the nanopores are nearly proportional to the volumetric fraction of incorporated  $\text{H}_2\text{SO}_4$  trapped in the GMs, which are confirmed by the theoretical estimation of the relation between the intersheet spacing and the packing density of GMs (Figure 4a).

GMs are composed of 3D wrinkled nanosheets and interlinked nanopores. It is difficult to identify their single microscopes and estimate their true pore sizes. However, several methods have been used to estimate their average pore sizes.<sup>36,44</sup> It is known that graphite is possibly the most compact



**Figure 4.** (a) Theoretical estimation of the relation between the pore diameter and the density of GM-SA-X, (b) XRD patterns of GM-SA-X, (c) nitrogen adsorption and desorption isotherms of GM-SA-X, and (d) pore size distributions of GM-SA-X.

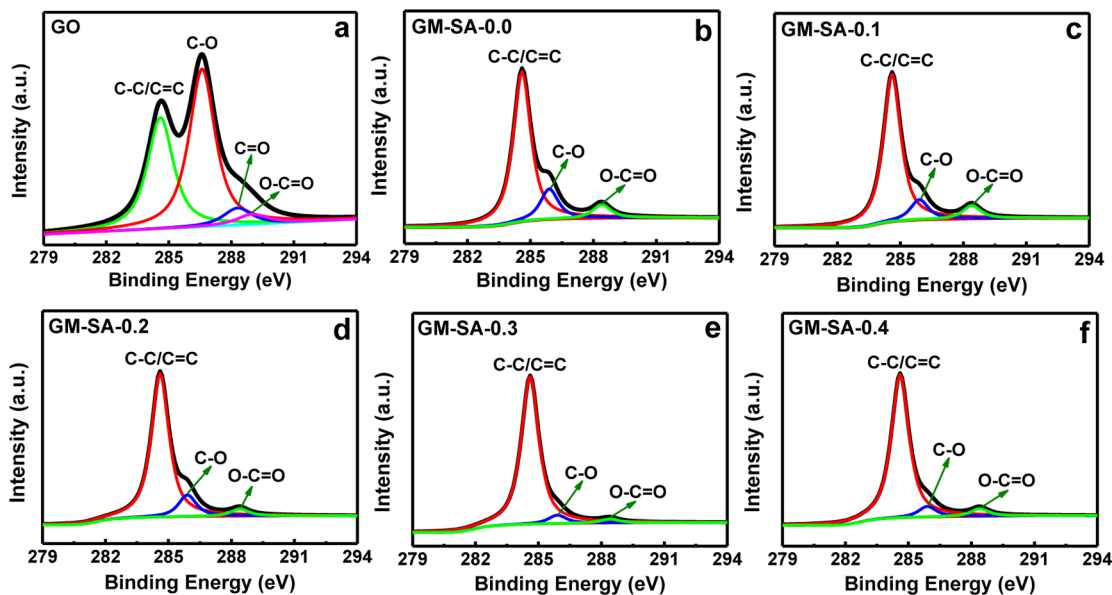


**Figure 5.** C 1s XPS spectra of (a) GO, (b) GM-SA-0.0, (c) GM-SA-0.1, (d) GM-SA-0.2, (e) GM-SA-0.3, and (f) GM-SA-0.4.

conductive carbon material with a density of  $2.2 \text{ g cm}^{-3}$  and the interplanar space of  $0.335 \text{ nm}$ .<sup>29,36</sup> Such small spaces prevent access of ions when graphite is used as the supercapacitor electrode. We propose that wrinkled graphene sheets are in a face-to-face arranged assembly,<sup>36,46</sup> thus the relationship of the interplanar space between the sheets and the packing density of GMs is given in Figure 4a. The packing density of GMs can be controlled in the range of  $0.27$ – $1.2 \text{ g cm}^{-3}$  when the concentration of  $\text{H}_2\text{SO}_4$  increases from  $0.4$  to

$0.0 \text{ mol L}^{-1}$ . The results are shown in the inset of Figure 4a. The retained  $\text{H}_2\text{SO}_4$  effectively separates the graphene sheets, and the interplanar spacing is about  $0.5$ – $4.8 \text{ nm}$  when the packing density changes from  $0.27$  to  $1.2 \text{ g cm}^{-3}$ . The structure and the interplanar spacing of the obtained GMs were further confirmed by XRD analyses as given in Figure 4b. A broad and weak (002) peak exists in each GM, which is obviously different from the sharp one of the graphite. The  $2\theta$  degree for the weak peaks has shifted apparently from  $25^\circ$  to  $21^\circ$  with the

increasing  $\text{H}_2\text{SO}_4$  concentration from 0.0 to 0.4 mol  $\text{L}^{-1}$ , corresponding to 0.39–0.6 nm of the  $d_{002}$  distance according to the Bragg equation ( $2d \sin \theta = n\lambda$ ).<sup>47</sup> More accurate information about the porous structure of GMs was obtained by nitrogen adsorption measurements, and the results were shown in Figure 4c. GM-SA-0.0 exhibits a Type I isotherm together with the characteristics of Type IV. Obvious micropore filling occurs at very low relative pressure, and the adsorption process quickly reaches a well-defined plateau. However, a very small but identifiable hysteresis loop indicates the existence of a very limited amount of mesopore. For comparison, with the increase of the concentration of  $\text{H}_2\text{SO}_4$ , a decreased adsorption amount at low pressure indicates a decrease of the micropore volume, while the appearance of a wide and more pronounced hysteresis loop is associated with a more developed mesopore. This result demonstrates that the higher the concentration of  $\text{H}_2\text{SO}_4$  solution remains, the larger the amount of mesopores GMs have. The pore distributions of GM-SA-X give more detailed information on the pore structure by the density functional theory (DFT) method based on nitrogen adsorption (Figure 4d). The samples display very narrow micro/mesopore size distributions with the average pore size located at 0.58, 1.7, 2.3, 3.4, to 4.8 nm for GM-SA-0.0, GM-SA-0.1, GM-SA-0.2, GM-SA-0.3, and GM-SA-0.4, respectively. Such results agree with the theoretical calculation shown in Figure 4a. Therefore, the porosity of the resultant GM can be tailored easily by  $\text{H}_2\text{SO}_4$  molecules as the separator. Depending on the different porous sizes, their supercapacitor performances of the resulting carbons may be changed.

To further illustrate the chemical composition of GMs, XPS has been performed as shown in Figure 5, and the detailed data for each C 1s peak are summarized in Table 1. As shown in

**Table 1. Contents of C and O in GMs from XPS Analysis**

sample	C–C/C=C [%]	C–O [%]	O–C=O [%]
	284.6 eV	285.9 eV	288.4 eV
GO	34.20	60.81	4.99
GM-SA-0.0	77.49	15.66	6.85
GM-SA-0.1	81.63	11.17	7.20
GM-SA-0.2	83.36	12.55	4.09
GM-SA-0.3	90.32	6.24	3.44
GM-SA-0.4	88.83	6.55	4.62

Figure 5, the peak at 284.6 eV corresponds to the C–C bond of the graphite carbon, and the peaks at 285.9 and 288.4 eV can be attributed to C–O and O–C=O groups, respectively. The C 1s spectrum of the original GO (Figure 5a) reveals that it consists of two main components arising from C–O and C=C/C–C groups and two minor components from C=O and O–C=O groups. For comparison, a significant decrease in the oxygen-containing functional groups of GM-SA-X is observed. As shown in Table 1, it is clearly seen that GO contains about 34.20% C–C/C=C group, 60.81% C–O group, and 4.99% O–C=O group. After hydrothermal treatment, the content of the C–C/C=C group in the GM-SA-0.0 sample increases to 77.49%, and  $\text{H}_2\text{SO}_4$ -mediated GMs show gradually increased content of the C–C/C=C group. A maximum content of the C–C/C=C group is achieved for GM-SA-0.3 with the content of 90.32%. A further increase of  $\text{H}_2\text{SO}_4$  concentration to 0.4 mol  $\text{L}^{-1}$  leads to a much lower C–C/C=C content (88.83%). The above results indicate that  $\text{H}_2\text{SO}_4$  can act as the catalyst for

removal of the oxygenic and hydric groups of GO through dehydration.<sup>41</sup>

Two-electrode supercapacitor cells were constructed to assess the electrochemical performances of  $\text{H}_2\text{SO}_4$ -mediated GMs in 1.0 mol  $\text{L}^{-1}$   $\text{H}_2\text{SO}_4$  electrolyte, as shown in Figure 6. The CV of each GM electrode displays a rectangular-like shape in the  $\text{H}_2\text{SO}_4$  electrolyte at a scan rate of 10  $\text{mV s}^{-1}$ , indicating the characteristic of electric double-layer capacitors (EDLCs) (Figure 6a).  $\text{H}_2\text{SO}_4$  contents in GMs play an important role in their capacitance, which increases qualitatively with increasing  $\text{H}_2\text{SO}_4$  content in the GM samples. This result is in good agreement with the order of the pore sizes of these samples, highlighting the advantage of the accessible porous structures for enhanced capacitance.

The galvanostatic charge/discharge curves at the current density of 0.1  $\text{A g}^{-1}$  were used to characterize the capacitive properties of  $\text{H}_2\text{SO}_4$ -mediated GMs as shown in Figure 6b. The linear shapes of GM samples in  $\text{H}_2\text{SO}_4$  electrolyte indicate the presence of EDLC, which is consistent with the CV results. In the acidic electrolyte, GM-SA-0.0 with the small pore size exhibits poor electrochemical capacitance. Figure 6c gives the relationships between  $C_s$  and current densities for  $\text{H}_2\text{SO}_4$ -mediated GMs. Over the current density in the range from 0.05 to 2.0  $\text{A g}^{-1}$  in 1 mol  $\text{L}^{-1}$   $\text{H}_2\text{SO}_4$  electrolyte, the charge storage capacities of the obtained samples quantitatively decrease in the following order: GM-SA-0.4 > GM-SA-0.3 > GM-SA-0.2 > GM-SA-0.1 > GM-SA-0.0, and  $C_s$  is 223, 213, 192, 163, and 126  $\text{F g}^{-1}$  at the current density of 1.0  $\text{A g}^{-1}$ , respectively. Such performances are in agreement with the character of the porous structures of these carbons, where the larger the pore size, the higher the charge storage capacity. Thus, the GM-SA-0.4 sample with the largest pore size (4.8 nm) presents the highest performance for 240, 230, 228, 225, 223, and 220  $\text{F g}^{-1}$  at the current density of 0.05, 0.1, 0.2, 0.5, 1.0, and 2.0  $\text{A g}^{-1}$ , respectively. The excellent high rate performance of the resultant GM-SA-0.4 is attributed to its mesoporous structure that facilitates rapid electrolyte transfer.<sup>27,29</sup> These values are significantly higher than 202  $\text{F g}^{-1}$  of previously reported chemically modified graphene (at 1.0  $\text{A g}^{-1}$ )<sup>48</sup> and 125.4  $\text{F g}^{-1}$  of activated carbon (at 0.1  $\text{A g}^{-1}$ )<sup>49</sup> and similar to 222  $\text{F g}^{-1}$  of the graphene hydrogel (at 1.0  $\text{A g}^{-1}$ ).<sup>40</sup> The superior electrochemical performance suggests that the porous structure of obtained GMs is favorable for their applications in supercapacitors.

To further understand the capacitive behaviors of the obtained GM samples, we performed EIS plots to ascertain the role of the preincorporated  $\text{H}_2\text{SO}_4$  electrolyte, as shown in Figure 6d. In the frequency range from 100 kHz to 10 mHz, a semicircle following a diagonal is observed for each sample. The semicircles in the high-frequency region reflect the existence of the charge transfer resistance, and their diameters are listed in the following order: GM-SA-0.0 > GM-SA-0.1 > GM-SA-0.2 > GM-SA-0.3 > GM-SA-0.4. Such decreasing diameters are in line with the increasing  $\text{H}_2\text{SO}_4$  contents, indicating a reduced trend of charge transfer resistance compared with the GM-SA-0.0 sample. The above results indicate that highly efficient ion transport channels are retained in  $\text{H}_2\text{SO}_4$ -mediated GMs.<sup>36</sup> Due to the fluid nature of liquid electrolyte, the continuous liquid network is likely to remain within the whole GM during the capillary compression process. To better reveal the electrochemical performances of  $\text{H}_2\text{SO}_4$ -mediated GMs, their Ragone plots are shown in Figure 6e. The energy density and power density of the supercapacitor devices are decreasing with

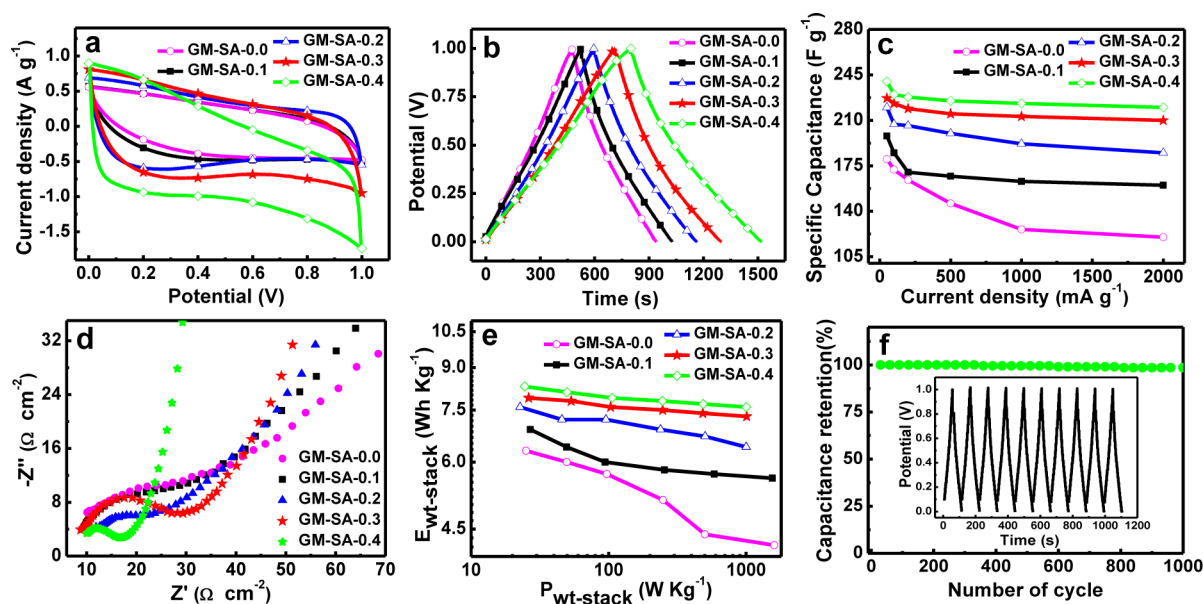


**Figure 6.** Electrochemical characterization of the two-electrode cell made from GM-SA-X in 1.0 mol L<sup>-1</sup> H<sub>2</sub>SO<sub>4</sub> (the concentration of SA from 0.0 to 0.4 mol L<sup>-1</sup>): (a) CV curves at 10 mV s<sup>-1</sup>, (b) charge and discharge profiles of GM-SA-X at the same current density of 0.1 A g<sup>-1</sup>, (c) gravimetric capacitances of samples at various current densities, (d) Nyquist plots of GM-SA-X electrodes, (e) Ragone plots of GM-SA-X, and (f) the cycling performance of GM-SA-X at 1.0 A g<sup>-1</sup>.

the reducing content of H<sub>2</sub>SO<sub>4</sub> in the GM samples. The GM-SA-0.4 sample shows the best electrochemical performance in these samples. Its energy density is up to 8.3 Wh kg<sup>-1</sup> at the power density of 24.5 W kg<sup>-1</sup>, and it still keeps 7.6 Wh kg<sup>-1</sup> even at the power density of 1000 W kg<sup>-1</sup>, highlighting the crucial role of the low ion transport resistance for achieving a high energy density. The GM-SA-0.4 sample is very stable under repeated charging/discharging for 1000 cycles (Figure 6f). Over 98.5% of the initial capacitance is retained at the current density of 1.0 A g<sup>-1</sup> in 1.0 mol L<sup>-1</sup> H<sub>2</sub>SO<sub>4</sub> electrolyte. Relying on these attractive features, the obtained graphene macroforms show very good prospects of practical applications in energy storage.

#### 4. CONCLUSION

Dense 3D graphene macroforms with nanotuned pore sizes have been prepared by the combination of hydrothermal method and evaporation process using GO as the precursors and aqueous H<sub>2</sub>SO<sub>4</sub> as the mediator. It is found that concentrated H<sub>2</sub>SO<sub>4</sub> trapped in the resultant carbons after evaporation of water plays an important role in the purity of the final graphene and the formation of the porous structures. It is found that H<sub>2</sub>SO<sub>4</sub> as the catalyst could remove the oxygenic and hydric groups of GO through dehydration. Furthermore, the pore sizes of H<sub>2</sub>SO<sub>4</sub>-mediated GMs can be tailored in the range of 0.5–4.8 nm by gradually increasing the concentration of H<sub>2</sub>SO<sub>4</sub> solution from 0.0 to 0.4 mol L<sup>-1</sup>. However, the 3D hydrogel is hard to form when the concentration of H<sub>2</sub>SO<sub>4</sub> is higher than 0.4 mol L<sup>-1</sup> because of the negative effect of strong acid conditions on the synthesis. Depending on the different porous sizes, 120–240 F g<sup>-1</sup> of specific capacity can be achieved for the obtained carbon samples. The GM-SA-0.4 sample with the pore size of 4.8 nm exhibits the outstanding specific capacitance in the wide range of charge–discharge rates and the highest electrochemical stability in H<sub>2</sub>SO<sub>4</sub> electrolyte. Its specific energy density and power density are, respectively, up to 8.3–7.6 Wh kg<sup>-1</sup> and about 24.5–1000 W kg<sup>-1</sup> in a two-

electrode cell, which are obviously superior to those of the reported carbonaceous materials. Different from the traditional hard and soft template methods for tailoring of the pore sizes of the carbons, this strategy presented here is a simple and effective way to produce high performance capacitor devices via controlling the pore size of the carbon electrodes. Furthermore, the shaped GMs are easy to fabricate the electrodes, and no additives are required due to their acceptable conductivity, which will provide a new idea for the large-scale assembly of supercapacitor devices.

#### ■ ASSOCIATED CONTENT

##### Supporting Information

The Supporting Information is available free of charge on the ACS Publications website at DOI: 10.1021/acs.jpcc.5b06616.

Additional experimental details and Figures S1–S4 (PDF)

#### ■ AUTHOR INFORMATION

##### Corresponding Authors

\*Tel.: +86-411-82158329. E-mail: qujy@lnnu.edu.cn.

\*Tel.: +86-532-86983452. E-mail: wumb@upc.edu.cn.

##### Notes

The authors declare no competing financial interest.

#### ■ ACKNOWLEDGMENTS

This work is supported by the NSFC (Nos. 51372277, 50902066), China Postdoctoral Science Foundation (2013M530922, 2014T70253), Program for Liaoning Excellent Talents in University (LJQ2014118), and the Fundamental Research Funds for the Central Universities (No.15CX08005A).

## REFERENCES

- (1) Kan, L. Y.; Xu, Z.; Gao, C. General avenue to individually dispersed graphene oxide-based two-dimensional molecular brushes by free radical polymerization. *Macromolecules* **2011**, *44*, 444–452.
- (2) Zhu, Y.; Murali, S.; Cai, W.; Li, X.; Suk, J. W.; Potts, J. R.; Ruoff, R. S. Graphene and graphene oxide: synthesis, properties, and applications. *Adv. Mater.* **2010**, *22*, 3906–3924.
- (3) Sun, Y. Q.; Wu, Q.; Shi, G. Q. Graphene based new energy materials. *Energy Environ. Sci.* **2011**, *4*, 1113–1132.
- (4) Chen, Z. P.; Ren, W. C.; Gao, L. B.; Liu, B. L.; Pei, S. F.; Cheng, H. M. Three-dimensional flexible and conductive interconnected graphene networks grown by chemical vapour deposition. *Nat. Mater.* **2011**, *10*, 424–428.
- (5) Deokar, G.; Avila, J.; Colombo, I. R.; Codron, J. L.; Boyaval, C.; Galopin, E.; Asensio, M. C.; Vignaud, D. Towards high quality CVD graphene growth and transfer. *Carbon* **2015**, *89*, 82–92.
- (6) He, Q. Y.; Wu, S. X.; Yin, Z. Y.; Zhang, H. Graphene-based electronic sensors. *Chem. Sci.* **2012**, *3*, 1764–1772.
- (7) Sun, Z. Z.; Yan, Z.; Yao, J.; Beitler, E.; Zhu, Y.; Tour, J. M. Growth of graphene from solid carbon sources. *Nature* **2010**, *468*, 549–552.
- (8) Li, W. W.; Gao, S.; Wu, L. Q.; Qiu, S. Q.; Guo, Y. F.; Geng, X. M.; Chen, M.; Liao, S.; Zhu, C.; Gong, Y.; et al. High-density three-dimension graphene macroscopic objects for high-capacity removal of heavy metal ions. *Sci. Rep.* **2013**, *3*, 2125.
- (9) Novoselov, K. S.; Geim, A. K.; Morozov, S. V.; Jiang, D.; Zhang, Y.; Dubonos, S. V.; Grigorieva, I. V.; Firsov, A. A. Electric field effect in atomically thin carbon films. *Science* **2004**, *306*, 666–669.
- (10) Dreyer, D. R.; Ruoff, R. S.; Bielawski, C. W. From conception to realization: an historical account of graphene and some perspectives for its future. *Angew. Chem., Int. Ed.* **2010**, *49*, 9336–9344.
- (11) Lui, C. H.; Liu, L.; Mak, K. F.; Flynn, G. W.; Heinz, T. F. Ultraflat graphene. *Nature* **2009**, *462*, 339–341.
- (12) Bai, H.; Li, C.; Shi, G. Q. Functional composite materials based on chemically converted graphene. *Adv. Mater.* **2011**, *23*, 1089–1115.
- (13) Lee, Y.; Kwon, J.; Hwang, E.; Ra, C. H.; Yoo, W. J.; Ahn, J. H.; Park, J. H.; Cho, J. H. High-performance perovskite–graphene hybrid photodetector. *Adv. Mater.* **2015**, *27*, 41–46.
- (14) Vickery, J. L.; Patil, A. J.; Mann, S. Fabrication of graphene-polymer nanocomposites with higher-order three-dimensional architectures. *Adv. Mater.* **2009**, *21*, 2180–2184.
- (15) Yu, H. L.; Ma, C.; Ge, B. H.; Chen, Y. J.; Xu, Z.; Zhu, C. L.; Li, C.; Ouyang, Q.; Gao, P.; Li, J.; et al. Three-dimensional hierarchical architectures constructed by graphene/MoS<sub>2</sub> nanoflake arrays and their rapid charging/discharging properties as lithium-ion battery anodes. *Chem. - Eur. J.* **2013**, *19*, 5818–5823.
- (16) Xu, Y. X.; Sheng, K. X.; Li, C.; Shi, G. Q. Self-assembled graphene hydrogel via a one-step hydrothermal process. *ACS Nano* **2010**, *4*, 4324–4330.
- (17) Zhu, S. Z.; Li, T. Hydrogenation-assisted graphene origami and its application in programmable molecular mass uptake, storage, and release. *ACS Nano* **2014**, *8*, 2864–2872.
- (18) Liu, H.; Wang, Y.; Gou, X.; Qi, T.; Yang, J.; Ding, Y. Three-dimensional graphene/polyaniline composite material for high-performance supercapacitor applications. *Mater. Sci. Eng., B* **2013**, *178*, 293–298.
- (19) Zhong, C.; Wang, J. Z.; Gao, X. W.; Wexler, D.; Liu, H. K. In situ one-step synthesis of a 3D nanostructured germanium-graphene composite and its application in lithium-ion batteries. *J. Mater. Chem. A* **2013**, *1*, 10798–10804.
- (20) Chen, W.; Yan, L. In situ self-assembly of mild chemical reduction graphene for three-dimensional architectures. *Nanoscale* **2011**, *3*, 3132–3137.
- (21) Jiang, X.; Ma, Y. W.; Li, J. J.; Fan, Q. L.; Huang, W. Self-assembly of reduced graphene oxide into three-dimensional architecture by divalent Ion linkage. *J. Phys. Chem. C* **2010**, *114*, 22462–22465.
- (22) Lee, S. H.; Kim, H. W.; Hwang, J. O.; Lee, W. J.; Kwon, J.; Bielawski, C. W.; Ruoff, R. S.; Kim, S. O. Three-dimensional self-assembly of graphene oxide platelets into mechanically flexible macroporous carbon films. *Angew. Chem., Int. Ed.* **2010**, *49*, 10084–10088.
- (23) Xu, Y. X.; Shi, G. Q. Assembly of chemically modified graphene: methods and applications. *J. Mater. Chem.* **2011**, *21*, 3311–3323.
- (24) Zhang, L. Y.; Zhang, L.; Zhang, J.; Xue, P.; Hao, W. W.; Shen, M.; Zheng, H. In situ growth of three-dimensional graphene coatings on arbitrary-shaped micro/nano materials and its mechanism studies. *Carbon* **2015**, *92*, 84–95.
- (25) Bi, H. C.; Yin, K. B.; Xie, X.; Zhou, Y. L.; Wan, N.; Xu, F.; Banhart, F.; Sun, L.; Ruoff, R. S. Low temperature casting of graphene with high compressive strength. *Adv. Mater.* **2012**, *24*, 5124–5129.
- (26) Hu, H.; Zhao, Z. B.; Wan, W. B.; Gogotsi, Y.; Qiu, J. S. Ultralight and highly compressible graphene aerogels. *Adv. Mater.* **2013**, *25*, 2219–2223.
- (27) Wu, Z. S.; Sun, Y.; Tan, Y. Z.; Yang, S.; Feng, X.; Mullen, K. Three-dimensional graphene-based macro- and mesoporous frameworks for high-performance electrochemical capacitive energy storage. *J. Am. Chem. Soc.* **2012**, *134*, 19532–19535.
- (28) Bai, H.; Li, C.; Wang, X. L.; Shi, G. Q. A pH-sensitive graphene oxide composite hydrogel. *Chem. Commun.* **2010**, *46*, 2376–2378.
- (29) Tao, Y.; Xie, X.; Lv, W.; Tang, D. M.; Kong, D.; Huang, Z.; Nishihara, H.; Ishii, T.; Li, B.; Golberg, D.; Kang, F.; Kyotani, T.; Yang, Q. H. Towards ultrahigh volumetric capacitance: graphene derived highly dense but porous carbons for supercapacitors. *Sci. Rep.* **2013**, *3*, 2975.
- (30) Xu, Z.; Zheng, B. N.; Chen, J. W.; Gao, C. Highly efficient synthesis of neat graphene nanoscrolls from graphene oxide by well-controlled lyophilization. *Chem. Mater.* **2014**, *26*, 6811–6818.
- (31) Xu, Z.; Zhang, Y.; Li, P.; Gao, C. Strong, conductive, lightweight, neat graphene aerogel fibers with aligned pores. *ACS Nano* **2012**, *6*, 7103–7113.
- (32) Xu, Z.; Sun, H. Y.; Gao, C. Perspective: Graphene aerogel goes to superelasticity and ultraflyweight. *APL Mater.* **2013**, *1*, 030901.
- (33) Liu, J. J.; Lv, W.; Wei, W.; Zhang, C.; Li, Z. J.; Li, B. H.; Kang, F.; Yang, Q. H. A three-dimensional graphene skeleton as a fast electron and ion transport network for electrochemical applications. *J. Mater. Chem. A* **2014**, *2*, 3031–3037.
- (34) Tang, Z. H.; Shen, S. L.; Zhuang, J.; Wang, X. Noble-metal-promoted three-dimensional macroassembly of single-layered graphene oxide. *Angew. Chem., Int. Ed.* **2010**, *49*, 4603–4607.
- (35) Tao, Y.; Kong, D. B.; Zhang, C.; Lv, W.; Wang, M. X.; Li, B. H.; Huang, Z. H.; Kang, F.; Yang, Q. H. Monolithic carbons with spheroidal and hierarchical pores produced by the linkage of functionalized graphene sheets. *Carbon* **2014**, *69*, 169–177.
- (36) Yang, X. W.; Cheng, C.; Wang, Y. F.; Qiu, L.; Li, D. Liquid-mediated dense integration of graphene materials for compact capacitive energy storage. *Science* **2013**, *341*, 534–537.
- (37) Lai, L. F.; Yang, H. P.; Wang, L.; Teh, B. K.; Zhong, J. Q.; Chou, H.; Chen, L.; Chen, W.; Shen, Z.; Ruoff, R. S.; et al. Preparation of supercapacitor electrodes through selection of graphene surface functionalities. *ACS Nano* **2012**, *6*, 5941–5951.
- (38) Xing, L. B.; Hou, S. F.; Zhou, J.; Li, S. J.; Zhu, T. T.; Li, Z. H.; Si, W.; Zhuo, S. UV-assisted photoreduction of graphene oxide into hydrogels high-rate capacitive performance in supercapacitor. *J. Phys. Chem. C* **2014**, *118*, 25924–25930.
- (39) Pei, S.; Zhao, J.; Du, J.; Ren, W.; Cheng, H. M. Direct reduction of graphene oxide films into highly conductive and flexible graphene films by hydrohalic acids. *Carbon* **2010**, *48*, 4466–4474.
- (40) Zhang, L.; Shi, G. Q. Preparation of highly conductive graphene hydrogels for fabricating supercapacitors with high rate capability. *J. Phys. Chem. C* **2011**, *115*, 17206–17212.
- (41) Hong, Y.; Wang, Z.; Jin, X. Sulfuric acid intercalated graphite oxide for graphene preparation. *Sci. Rep.* **2013**, *3*, 3439.
- (42) Qu, J. Y.; Shi, L.; He, C. X.; Gao, F.; Li, B. B.; Zhou, Q.; Hu, H.; Shao, G. H.; Wang, X. Z.; Qiu, J. S. Highly efficient synthesis of graphene/MnO<sub>2</sub> hybrids and their application for ultrafast oxidative decomposition of methylene blue. *Carbon* **2014**, *66*, 485–492.

(43) Qu, J. Y.; Gao, F.; Zhou, Q.; Wang, Z. Y.; Hu, H.; Li, B. B.; Wan, W. B.; Wang, X. Z.; Qiu, J. S. Highly atom-economic synthesis of graphene/Mn<sub>3</sub>O<sub>4</sub> hybrid composites for electrochemical supercapacitors. *Nanoscale* **2013**, *5*, 2999–3005.

(44) Wu, M. B.; Li, P.; Li, Y.; Liu, J.; Wang, Y. Enteromorpha based porous carbons activated by zinc chloride for supercapacitors with high capacity retention. *RSC Adv.* **2015**, *5*, 16575–16581.

(45) Wu, M. B.; Ai, P. p.; Tan, M. H.; Jiang, B.; Li, Y. P.; Zheng, J. T.; Wu, W.; Li, Z.; Zhang, Q.; He, X. Synthesis of starch-derived mesoporous carbon for electric double layer capacitor. *Chem. Eng. J.* **2014**, *245*, 166–172.

(46) Geim, A. K.; Novoselov, K. S. The rise of graphene. *Nat. Mater.* **2007**, *6*, 183–191.

(47) Li, L. H.; Wu, Y. E.; Lu, J.; Nan, C. Y.; Li, Y. D. Synthesis of Pt-Ni-graphene via in situ reduction and its enhanced catalyst activity for the methanol oxidation. *Chem. Commun.* **2013**, *49*, 7486–7488.

(48) Choi, B. G.; Yang, M.; Hong, W. H.; Choi, J.; Huh, Y. S. 3D macroporous graphene frameworks for supercapacitors with high energy and power density. *ACS Nano* **2012**, *6*, 4020–4028.

(49) He, X. J.; Geng, Y. J.; Qiu, J. S.; Zheng, M. D.; Long, S.; Zhang, X. Y. Effect of activation time on the properties of activated carbons prepared by microwave-assisted activation for electric double layer capacitors. *Carbon* **2010**, *48*, 1662–1669.